Journal of Sound and Vibration (2002) **257**(2), 283–299
doi:10.1006/jsvi.2001.3835, available online at http://www.idealibrary.com on IDEAL®

VIBRATIONAL POWER TRANSMISSION FROM A MACHINE TO ITS SUPPORTING CYLINDRICAL SHELL

W. L. Li and M. Daniels

United Technologies Research Center, 411 *Silver Lane*, *MS* 129-17, *East Hartford*, *CT* 06108, *U.S.A.*
E-mail: *liw@utrc.utc.com*

and

W. Zhou

United Technologies Carrier Corporation, *Carrier Parkway*, *Syracuse*, *NY* 13221, *U.S.A.*

(*Received* 18 *January* 2001, *and in final form* 11 *May* 2001)

Power flows from a vibratory machine to its supporting structure are of primary concern in a passive or active isolation system design. Although in the literature there is a fair number of investigations on the power inputs to beams, plates or the like, few attempts have been made for other commonly used structures such as cylindrical shells. In this paper, the vibratory power flows from a rigid-body machine to an elastic cylindrical shell are studied considering the contributions of the non-radial (tangential and axial) displacements and forces. In particular, it is argued that the notion that the motion of a thin shell is primarily radial does not necessarily dictate that the power transmissions are predominantly carried out by the radial displacement. This point is subsequently illuminated through numerical examples. Another issue discussed here is concerned with the effects on the power flows of the cross couplings of the (different) displacement components. It is shown that even though the contributions of the cross couplings are usually insignificant, they may become important if the vibration isolators are substantially hard as compared with the local shell stiffness or impedance. This assertion is particularly useful when an experimental technique is used to measure the vibratory power flows into a supporting structure.

1. INTRODUCTION

The reaction forces (or force transmissibility functions) are often used to measure the performance of an isolation system. However, since the reaction forces at each isolator location are typically different in terms of phase and direction, one may find it difficult to directly use them to define an objective or cost function for the purpose of design optimization. This problem is further compounded by the fact that the magnitudes of the reaction forces are not necessarily a sensitive gauge of the severity of the vibrations on the receiving structure. Recently, vibrational power flows from a machine into its supporting structure have been widely used to assess the effectiveness of passive and active vibration isolation systems [1–10]. Gardonio *et al.* [11, 12] compared the minimization of total power transmission with several other active control strategies such as the cancellation of out-of-plane forces. It is concluded that the control of total power gives the best results under ideal conditions. The importance of considering the power flows associated with the rotational displacements (or alternatively, isolator rotational stiffnesses or moment excitations) are discussed in references [13–16], where it is shown that the power flows associated with the rotational displacements tend to become more important as frequency increases.

0022-460X/02/$35.00

It should be pointed out that the receiving or supporting structures involved in these investigations are mostly beams, plates or the like. Howard *et al.* [9] studied the power transmission from a vibrating rigid body into a thin supporting cylindrical shell through a set of passive and active isolators. It is demonstrated that the real power transmitted into the supporting shell can be substantially reduced by employing, in parallel with existing passive isolators, active isolators adjusted to provide appropriate control forces. While their work is important and definitely useful to other researchers, it may have two flaws. The first one is that the axial and tangential displacements of the shell are assumed to be small enough to allow the corresponding forces and their related power transmissions to be ignored in the subsequent calculations. Secondly, only the odd modes (for the simple shell) are used to represent the radial displacement and the impact of the even modes is incorrectly considered by repeating the calculations simply with the co-ordinate system rotated 90° in the positive circumferential direction. In this study, these two problems are first corrected in the formulation. It is then demonstrated that the non-radial displacements can be as important as the radial displacement in conveying vibrational powers when a load is not applied primarily in the radial direction. The impact of the cross coupling of different displacement components is also discussed with necessary details.

2. DYNAMIC DESCRIPTION OF A COMPOSITE ISOLATION SYSTEM

2.1. THE MOTION OF A RIGID-BODY MACHINE

Figure 1 shows a vibratory machine that is mounted onto a circular cylindrical shell through multiple vibration isolators. It is assumed that the machine is subject to a set of prescribed loads such as force, moment and their combinations. In this study, the machine will be modelled as a rigid body, which is usually a valid simplification when the first natural frequency of the machine (structure) is significantly (say, twice) higher than the upper bound of the frequency range of interest. In dynamics, a rigid body is characterized by a 6×6 mass matrix

$$\mathbf{M} = \begin{bmatrix} m & 0 & 0 & 0 & 0 & 0 \\ 0 & m & 0 & 0 & 0 & 0 \\ 0 & 0 & m & 0 & 0 & 0 \\ 0 & 0 & 0 & I_{xx} & -I_{xy} & -I_{xz} \\ 0 & 0 & 0 & -I_{yx} & I_{yy} & -I_{yz} \\ 0 & 0 & 0 & -I_{zx} & -I_{zy} & I_{zz} \end{bmatrix}, \tag{1}$$

where m is the mass of the machine, and $I_{xx}, I_{yy}, \ldots, I_{yz}$ are the moments of inertia. A list of symbols is given in Appendix B.

The differential equation for the motion of the rigid body can be written as

$$\mathbf{M}\ddot{\mathbf{u}}^c = \mathbf{f}^m + \sum_{i=1}^{N_k} \mathbf{R}_i^c, \tag{2}$$

where $\mathbf{u}^c$ is the displacement vector of the center of gravity (CG) of the machine, $\mathbf{R}_i^c$ is the load vector resulting from the reaction forces at the ith mounting point, $\mathbf{f}$ represents all the other forces applied on the machine, and N_k denotes the total number of isolators.

The displacements at any mounting point can be directly obtained from

$$\mathbf{u}_i = \mathbf{G}_i \mathbf{u}^c, \tag{3}$$

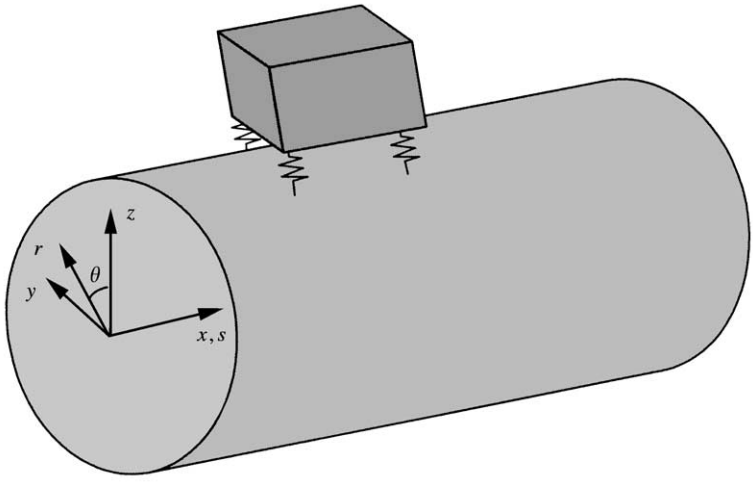

Figure 1. Schematic of a composite vibration isolation system.

where

$$\mathbf{G}_i = \begin{bmatrix} 1 & 0 & 0 & 0 & a_z^i & -a_y^i \\ 0 & 1 & 0 & -a_z^i & 0 & a_x^i \\ 0 & 0 & 1 & a_y^i & -a_x^i & 0 \\ 0 & 0 & 0 & 1 & 0 & 0 \\ 0 & 0 & 0 & 0 & 1 & 0 \\ 0 & 0 & 0 & 0 & 0 & 0 \end{bmatrix} \tag{4}$$

with a_x^i, a_y^i and a_z^i being, respectively, the projections onto x-, y- and z-axis of the distance (vector) from the machine CG to the ith isolator.

In this study, each isolator will be modelled as a lumped stiffness element with a negligible mass. Then, the reaction forces at the ith isolator location can be expressed as

$$\mathbf{R}_i = -\mathbf{K}_i(\mathbf{u}_i - \mathbf{u}_i^0) \tag{5}$$

or, by making use of equation (3),

$$\mathbf{R}_i = -\mathbf{K}_i(\mathbf{G}_i\mathbf{u}^c - \mathbf{u}_i^0), \tag{6}$$

where $\mathbf{K}_i$ is the stiffness matrix for the ith isolator, and $\mathbf{u}_i$ and $\mathbf{u}_i^0$ are, respectively, the displacement vectors at its upper and lower ends.

The stiffness matrix $\mathbf{K}_i$ is generally a 6×6 symmetric semi-positive definite matrix whose off-diagonal elements represent the cross coupling between different components. Mathematically, however, such a matrix can always be reduced, via orthogonal transformations, to a diagonal matrix whose diagonal elements are the principal (stiffness) values of the ith isolator. Thus, without loss of generality, the stiffness matrix $\mathbf{K}_i$ will be here represented by six simple springs in the principal directions. If p, q and r denote the three principal axes, then one has

$$\mathbf{K}_i = \hat{\mathbf{T}}_i^{\mathrm{T}} \operatorname{diag}(K_i^p, K_i^q, K_i^r, K_i'^p, K_i'^q, K_i'^r)\hat{\mathbf{T}}_i, \tag{7}$$

where diag$(\cdot)$ denotes the diagonal matrix, K_i^j and $K_i'^j$ $(j = p, q, r)$ are, respectively, the stiffnesses of the linear and the rotational springs in the j direction, and

$$\hat{\mathbf{T}}_i = \begin{bmatrix} \mathbf{T}_i & \mathbf{0} \\ \mathbf{0} & \mathbf{T}_i \end{bmatrix} \tag{8}$$

with

$$\mathbf{T}_i = \begin{bmatrix} \lambda_{px}^i & \lambda_{py}^i & \lambda_{pz}^i \\ \lambda_{qx}^i & \lambda_{qy}^i & \lambda_{qz}^i \\ \lambda_{rx}^i & \lambda_{ry}^i & \lambda_{rz}^i \end{bmatrix} \tag{9}$$

being a transformation matrix whose elements are simply the direction cosines of the principal axes [10].

The (reaction) forces at each mounting point can be easily transferred to the CG of the rigid body, that is,

$$\mathbf{R}_i^c = \mathbf{G}_i^{\mathrm{T}} \mathbf{R}_i. \tag{10}$$

Substituting equations (6) and (10) into equation (2) results in

$$\bar{\mathbf{K}}\mathbf{u}^c + \mathbf{M}\ddot{\mathbf{u}}^c = \mathbf{f} + \sum_{i=1}^{N_k} \mathbf{K}_i^g \mathbf{u}_i^0, \tag{11}$$

where

$$\bar{\mathbf{K}} = \sum_{i=1}^{N_k} \mathbf{G}_i^{\mathrm{T}} \mathbf{K}_i \mathbf{G}_i, \qquad \mathbf{K}_i^g = \mathbf{G}_i^{\mathrm{T}} \mathbf{K}_i. \tag{12, 13}$$

If the vibrations of the supporting structure are so small that the corresponding forces, $\sum_{i=1}^{N_i} \mathbf{K}_i^g \mathbf{u}_i^0$, are essentially negligible compared to the external force $\mathbf{f}$, equation (11) alone can be used to solve for the motion of the machine as in a traditional vibration isolation analysis. Otherwise, the solution cannot be independently obtained without explicitly knowing the motions of the supporting structure at the mounting points. Thus, the motions of the machine and supporting structure are now coupled together and have to be determined simultaneously.

2.2. VIBRATION OF A CIRCULAR CYLINDRICAL SHELL

Assume that the supporting structure is a circular cylindrical shell of mean radius R, thickness h and length L. If u, v, and w, respectively, denote the displacements in the axial x, circumferential θ and radial r directions, then the equations of the motions of the shell can be written as

$$\frac{\partial^2 u}{\partial s^2} + \frac{1-\nu}{2}\frac{\partial^2 u}{\partial \theta^2} + \frac{1+\nu}{2}\frac{\partial^2 v}{\partial s\,\partial \theta} + \nu\frac{\partial w}{\partial s} = \frac{\rho(1-\nu^2)R^2}{E}\frac{\partial^2 u}{\partial t^2} - \frac{(1-\nu^2)}{Eh}p_s, \tag{14a}$$

$$\frac{1+\nu}{2}\frac{\partial^2 u}{\partial s\,\partial \theta} + \frac{(1-\nu)}{2}\frac{\partial^2 v}{\partial s^2} + \frac{\partial^2 v}{\partial \theta^2} + \kappa\left(2(1-\nu)\frac{\partial^2 v}{\partial s^2} + \frac{\partial^2 v}{\partial \theta^2}\right) + \frac{\partial w}{\partial \theta} - \kappa\left((2-\nu)\frac{\partial^3 w}{\partial s^2\,\partial \theta} + \frac{\partial^3 w}{\partial \theta^3}\right)$$
$$= \frac{\rho(1-\nu^2)R^2}{E}\frac{\partial^2 v}{\partial t^2} - \frac{(1-\nu^2)}{Eh}p_\theta, \tag{14b}$$

$$\nu\frac{\partial u}{\partial s} + \frac{\partial v}{\partial \theta} - \kappa\left((2-\nu)\frac{\partial^3 v}{\partial s^2\,\partial \theta} + \frac{\partial^3 v}{\partial \theta^3}\right) + w + \kappa\nabla^4 w = -\frac{\rho(1-\nu^2)R^2}{E}\frac{\partial^2 w}{\partial t^2} + \frac{(1-\nu^2)}{Eh}p_r, \tag{14c}$$

where E, v and ρ are, respectively, Young's modulus, the Poisson ratio and the mass density of the shell material; p_s, p_θ and p_r are, respectively, the distributed forces in $s\,(=x/R)$, θ and r directions; and $\kappa = h^2/12R^2$. Instead of the popular Donnell–Mushtari equations, here the Goldenveizer–Novozhilov (also Arnold–Warburton) equations are used to determine the shell vibrations since the Goldenveizer–Novozhilov equations are often found more accurate in predicting the modal properties of a shell [17].

Once the three independent displacements, u, v, and w, are obtained from equation (14), the displacement vector at any point on the shell can be readily calculated from

$$\mathbf{U} = \left\{u, v, w, \frac{1}{R}\frac{\partial w}{\partial \theta} - \frac{v}{R}, -\frac{1}{R}\frac{\partial w}{\partial s}, \frac{1}{2R}\left(\frac{\partial v}{\partial s} - \frac{\partial u}{\partial \theta}\right)\right\}. \tag{15}$$

The last three components in equation (15) represent the rotations about the x-, θ- and r axis, respectively.

Let $\tilde{\mathbf{R}}_i$ be the forces at the ith isolator, the distributed forces on the right-hand side of equation (14) can be expressed as [18]

$$p_s = \sum_{i=1}^{N_k} \left\{\delta(s - s_i, \theta - \theta_i), 0, 0, 0, 0, \frac{\partial\delta(s - s_i, \theta - \theta_i)}{2R\,\partial\theta}\right\}\tilde{\mathbf{R}}_i, \tag{16a}$$

$$p_\theta = \sum_{i=1}^{N_k} \left\{0, \delta(s - s_i, \theta - \theta_i), 0, -\frac{\delta(s - s_i, \theta - \theta_i)}{R}, 0, -\frac{\partial\delta(s - s_i, \theta - \theta_i)}{2R\,\partial s}\right\}\tilde{\mathbf{R}}_i \tag{16b}$$

and

$$p_r = \sum_{i=1}^{N_k} \left\{0, 0, \delta(s - s_i, \theta - \theta_i), -\frac{\partial\delta(s - s_i, \theta - \theta_i)}{R\,\partial\theta}, \frac{\partial\delta(s - s_i, \theta - \theta_i)}{R\,\partial s}, 0\right\}\tilde{\mathbf{R}}_i. \tag{16c}$$

As often done in a response analysis for a simple shell, the displacements will be here sought in the following forms:

$$u(s, \theta, t) = e^{i\omega t} \sum_{m=1}^{M}\sum_{n=0}^{N-1} [a_{mn}\cos\lambda_m s\cos n\theta + b_{mn}\cos\lambda_m s\sin n\theta] \quad (\lambda_m = m\pi R/L), \tag{17a}$$

$$v(s, \theta, t) = e^{i\omega t} \sum_{m=1}^{M}\sum_{n=0}^{N-1} [c_{mn}\sin\lambda_m s\cos n\theta + d_{mn}\sin\lambda_m s\sin n\theta] \tag{17b}$$

and

$$w(s, \theta, t) = e^{i\omega t} \sum_{m=1}^{M}\sum_{n=0}^{N-1} [e_{mn}\sin\lambda_m s\cos n\theta + f_{mn}\sin\lambda_m s\sin n\theta]. \tag{17c}$$

Substituting equation (17) into equation (14) and making use of the orthogonality of the trigonometric functions result in

$$\left\{\begin{bmatrix}\bar{A}^s & \mathbf{0}\\ \mathbf{0} & \bar{A}^a\end{bmatrix} - \omega^2 m_s\begin{bmatrix}\mathbf{I} & \mathbf{0}\\ \mathbf{0} & \mathbf{I}\end{bmatrix}\right\}\begin{bmatrix}\bar{\mathbf{a}}^s\\ \bar{\mathbf{a}}^a\end{bmatrix} = \begin{bmatrix}\bar{\mathbf{p}}^s\\ \bar{\mathbf{p}}^a\end{bmatrix}, \tag{18}$$

where

$$\bar{\Lambda}^s = \begin{bmatrix} \Lambda^{ss} & \Lambda^{s\theta} & \Lambda^{sr} \\ \Lambda^{s\theta^{\mathrm{T}}} & \Lambda^{\theta\theta} & \Lambda^{\theta r} \\ \Lambda^{sr^{\mathrm{T}}} & \Lambda^{\theta r^{\mathrm{T}}} & \Lambda^{rr} \end{bmatrix}, \qquad \bar{\Lambda}^a = \begin{bmatrix} \Lambda^{ss} & -\Lambda^{s\theta} & \Lambda^{sr} \\ -\Lambda^{s\theta^{\mathrm{T}}} & \Lambda^{\theta\theta} & -\Lambda^{\theta r} \\ \Lambda^{sr^{\mathrm{T}}} & -\Lambda^{\theta r^{\mathrm{T}}} & \Lambda^{rr} \end{bmatrix}, \tag{19a, b}$$

$$\bar{\mathbf{p}}^{\alpha}_{mn} = \{\bar{p}^{\alpha}_{s,mn}, \bar{p}^{\alpha}_{\theta,mn}, \bar{p}^{\alpha}_{r,mn}\}^{\mathrm{T}} \quad (\alpha = s, a), \tag{19c}$$

$$\bar{\mathbf{a}}^{s}_{mn} = \{a_{mn}, d_{mn}, e_{mn}\}^{\mathrm{T}}, \qquad \bar{\mathbf{a}}^{a}_{mn} = \{b_{mn}, c_{mn}, f_{mn}\}^{\mathrm{T}} \tag{19d, e}$$

and $m_s = 2\pi RhL\rho/4$. For conciseness, the definitions of the sub-matrices and sub-vectors in equations (19) are given in Appendix A.

The force terms on the right-hand side of equation (18) attribute to the reaction forces that are dependent upon the relative motions between the machine and the shell at the isolator locations. Therefore, equations (18) and (11) are actually coupled together and have to be solved simultaneously for the vibrations of the machine and shell.

2.3. THE COUPLED EQUATIONS FOR THE MACHINE AND SHELL

For the sake of convenience, the Cartesian and cylindrical co-ordinate systems have been, respectively, used in describing the motions of the machine and shell. However, the relationship between these two co-ordinate systems can be readily established in terms of an orthogonal transformation matrix. Let $\bar{\mathbf{U}}_i$ be the displacement vector at the ith isolator location in the cylindrical co-ordinate system. Then, its counterpart in the Cartesian co-ordinate system can be expressed as

$$\mathbf{u}^0_i = \mathbf{Q}_i \bar{\mathbf{U}}_i, \tag{20}$$

where

$$\mathbf{Q}_i = \begin{bmatrix} \hat{\mathbf{Q}}_i & \mathbf{0} \\ \mathbf{0} & \hat{\mathbf{Q}}_i \end{bmatrix}, \qquad \hat{\mathbf{Q}}_i = \begin{bmatrix} 1 & 0 & 0 \\ 0 & \cos\theta_i & \sin\theta_i \\ 0 & -\sin\theta_i & \cos\theta_i \end{bmatrix}. \tag{21, 22}$$

Similarly, the forces applied to the shell by the ith isolator can be obtained from

$$\tilde{\mathbf{R}}_i = -\mathbf{Q}^{\mathrm{T}}_i \mathbf{R}_i \tag{23}$$

or

$$\tilde{\mathbf{R}}_i = \mathbf{Q}^{\mathrm{T}}_i \mathbf{K}_i \mathbf{G}_i \mathbf{u}^c - \mathbf{Q}^{\mathrm{T}}_i \mathbf{K}_i \mathbf{Q}_i \bar{\mathbf{U}}_i. \tag{24}$$

According to equation (15), one has

$$\bar{\mathbf{U}}_i = \left\{ u, v, w, \frac{1}{R}\frac{\partial w}{\partial \theta} - \frac{v}{R}, -\frac{1}{R}\frac{\partial w}{\partial x}, \frac{1}{2R}\left(\frac{\partial v}{\partial x} - \frac{\partial u}{\partial \theta}\right) \right\}^{\mathrm{T}} \Bigg|_{s=s_i,\, \theta=\theta_i} \tag{25}$$

or

$$\bar{\mathbf{U}}_i = \bar{\mathbf{U}}_{is} + \bar{\mathbf{U}}_{i\theta} + \bar{\mathbf{U}}_{ir}, \tag{26}$$

where

$$\bar{\mathbf{U}}_{is} = \left\{u, 0, 0, 0, 0, \frac{-1}{2R}\frac{\partial u}{\partial \theta}\right\}^{\mathrm{T}}\Big|_{s=s_i,\,\theta=\theta_i}, \qquad \bar{\mathbf{U}}_{i\theta} = \left\{0, v, 0, -\frac{v}{R}, 0, \frac{1}{2R}\frac{\partial v}{\partial s}\right\}^{\mathrm{T}}\Big|_{s=s_i,\,\theta=\theta_i} \tag{27a, b}$$

and

$$\bar{\mathbf{U}}_{ir} = \left\{0, 0, w, \frac{1}{R}\frac{\partial w}{\partial \theta}, -\frac{1}{R}\frac{\partial w}{\partial s}, 0\right\}^{\mathrm{T}}\Big|_{s=s_i,\,\theta=\theta_i}. \tag{27c}$$

In light of equations (17), equation (26) can be rewritten as

$$\bar{\mathbf{U}}_i = \sum_{m=1}^{M}\sum_{n=0}^{N-1}\left[\{\mathbf{U}^s_{i,mn}, \mathbf{V}^s_{i,mn}, \mathbf{W}^s_{i,mn}\}\bar{\mathbf{a}}^s_{mn} + \{\mathbf{U}^a_{i,mn}, \mathbf{V}^a_{i,mn}, \mathbf{W}^a_{i,mn}\}\bar{\mathbf{a}}^a_{mn}\right], \tag{28}$$

where

$$\mathbf{U}^s_{i,mn} = \left\{\cos\lambda_m s\cos n\theta, 0, 0, 0, 0, -\frac{1}{2R}\frac{\partial(\cos\lambda_m s\cos n\theta)}{\partial\theta}\right\}^{\mathrm{T}}\Big|_{s=s_i,\,\theta=\theta_i}, \tag{29a}$$

$$\mathbf{V}^s_{i,mn} = \left\{0, \sin\lambda_m s\sin n\theta, 0, -\frac{\sin\lambda_m s\sin n\theta}{R}, 0, \frac{1}{2R}\frac{\partial(\sin\lambda_m s\sin n\theta)}{\partial s}\right\}^{\mathrm{T}}\Big|_{s=s_i,\,\theta=\theta_i}, \tag{29b}$$

$$\mathbf{W}^s_{i,mn} = \left\{0, 0, \sin\lambda_m s\cos n\theta, \frac{1}{R}\frac{\partial(\sin\lambda_m s\sin n\theta)}{\partial\theta}, -\frac{1}{R}\frac{\partial(\sin\lambda_m s\cos n\theta)}{\partial s}, 0\right\}^{\mathrm{T}}\Big|_{s=s_i,\,\theta=\theta_i}, \tag{29c}$$

and $\mathbf{U}^a_{i,mn}$, $\mathbf{V}^a_{i,mn}$ and $\mathbf{W}^a_{i,mn}$ can be obtained from equations (29) by simply replacing $\cos n\theta$ and $\sin n\theta$ with $\sin n\theta$ and $\cos n\theta$ respectively.

Combining equations (16), (24) and (28) with equation (18) results in

$$\left\{\begin{bmatrix}\mathbf{\Lambda} + \bar{\mathbf{A}}^{ss} & \bar{\mathbf{A}}^{sa}\\ \bar{\mathbf{A}}^{sa\mathrm{T}} & \mathbf{\Lambda} + \bar{\mathbf{A}}^{aa}\end{bmatrix} - \omega^2 m_s\begin{bmatrix}\mathbf{I} & 0\\ 0 & \mathbf{I}\end{bmatrix}\right\}\begin{bmatrix}\bar{\mathbf{a}}_s\\ \bar{\mathbf{a}}_a\end{bmatrix} = \begin{bmatrix}\mathbf{H}_s\\ \mathbf{H}_a\end{bmatrix}\mathbf{u}^c, \tag{30}$$

$$\bar{\mathbf{A}}^{\alpha\beta} = \begin{bmatrix}\mathbf{A}^{\alpha\beta} & \mathbf{D}^{\alpha\beta} & \mathbf{E}^{\alpha\beta}\\ \mathbf{D}^{\alpha\beta\mathrm{T}} & \mathbf{B}^{\alpha\beta} & \mathbf{F}^{\alpha\beta}\\ \mathbf{E}^{\alpha\beta\mathrm{T}} & \mathbf{F}^{\alpha\beta\mathrm{T}} & \mathbf{C}^{\alpha\beta}\end{bmatrix}, \qquad \mathbf{H}_{\alpha,mn} = \sum_{i=1}^{N_k}\begin{bmatrix}\mathbf{U}^{\alpha}_{i,mn}\\ \mathbf{V}^{\alpha}_{i,mn}\\ \mathbf{W}^{\alpha}_{i,mn}\end{bmatrix}\mathbf{Q}_i^{\mathrm{T}}\mathbf{K}_i\mathbf{G}_i \quad (\alpha, \beta = s, a), \tag{31a, b}$$

where

$$A^{\alpha\beta}_{mn,mn'} = \sum_{i=1}^{N_k}(\mathbf{U}^{\alpha}_{i,mn})^{\mathrm{T}}\mathbf{Q}_i^{\mathrm{T}}\mathbf{K}_i\mathbf{Q}_i\mathbf{U}^{\beta}_{i,m'n'}, \qquad D^{\alpha\beta}_{mn,mn'} = \sum_{i=1}^{N_k}(\mathbf{U}^{\alpha}_{i,mn})^{\mathrm{T}}\mathbf{Q}_i^{\mathrm{T}}\mathbf{K}_i\mathbf{Q}_i(\mathbf{V}^{\beta}_{i,m'n'})^{\mathrm{T}}, \tag{32a, b}$$

$$E^{\alpha\beta}_{mn,mn'} = \sum_{i=1}^{N_k}(\mathbf{U}^{\alpha}_{i,mn})^{\mathrm{T}}\mathbf{Q}_i^{\mathrm{T}}\mathbf{K}_i\mathbf{Q}_i(\mathbf{W}^{\beta}_{i,m'n'})^{\mathrm{T}}, \qquad B^{\alpha\beta}_{mn,mn'} = \sum_{i=1}^{N_k}(\mathbf{V}^{\alpha}_{i,mn})^{\mathrm{T}}\mathbf{Q}_i^{\mathrm{T}}\mathbf{K}_i\mathbf{Q}_i\mathbf{V}^{\beta}_{i,mn}, \tag{32c, d}$$

$$F^{\alpha\beta}_{mn,mn'} = \sum_{i=1}^{N_k}(\mathbf{V}^{\alpha}_{i,mn})^{\mathrm{T}}\mathbf{Q}_i^{\mathrm{T}}\mathbf{K}_i\mathbf{Q}_i\mathbf{W}^{\beta}_{i,mn}, \qquad C^{\alpha\beta}_{mn,mn'} = \sum_{i=1}^{N_k}(\mathbf{W}^{\alpha}_{i,mn})^{\mathrm{T}}\mathbf{Q}_i^{\mathrm{T}}\mathbf{K}_i\mathbf{Q}_i\mathbf{W}^{\beta}_{i,mn}. \tag{32e, f}$$

Similarly, making using of equations (20) and (28), equation (11) can be rewritten as

$$\bar{\mathbf{K}}\mathbf{u}^c - \omega^2\mathbf{M}\mathbf{u}^c = \mathbf{f} + \{\mathbf{H}_s^{\mathrm{T}}, \mathbf{H}_s^{\mathrm{T}}\}\begin{bmatrix}\bar{\mathbf{a}}^s\\ \bar{\mathbf{a}}^a\end{bmatrix}. \tag{33}$$

Finally, combining equations (30) and (33) will lead to a coupled equation:

$$\left\{\begin{bmatrix}\bar{\mathbf{K}} & -\mathbf{H}_s^{\mathrm{T}} & -\mathbf{H}_a^{\mathrm{T}}\\ -\mathbf{H}_s & \bar{\mathbf{\Lambda}}^a + \bar{\mathbf{A}}^{ss} & \bar{\mathbf{A}}^{sa}\\ -\mathbf{H}_a & \bar{\mathbf{A}}^{sa\mathrm{T}} & \bar{\mathbf{\Lambda}}^a + \bar{\mathbf{A}}^{aa}\end{bmatrix} - \omega^2\begin{bmatrix}\mathbf{M} & \mathbf{0} & \mathbf{0}\\ \mathbf{0} & m_s\mathbf{I} & \mathbf{0}\\ \mathbf{0} & \mathbf{0} & m_s\mathbf{I}\end{bmatrix}\right\}\begin{bmatrix}\mathbf{u}^c\\ \bar{\mathbf{a}}_s\\ \bar{\mathbf{a}}_a\end{bmatrix} = \begin{bmatrix}\mathbf{f}\\ \mathbf{0}\\ \mathbf{0}\end{bmatrix}. \tag{34}$$

Clearly, the modal properties and the responses (to a given load) of the composite isolation system can now be readily determined from equation (34). Since equation (34) is often repeatedly solved at many frequency steps, the modal superposition technique will be employed in the subsequent calculations.

It is evident from equation (34) that the contributions of the odd and even modes can no longer be separated mathematically due to the presence of the isolators manifested in the off-diagonal matrices. In other words, the overall response cannot be generally obtained by independently expressing the displacements as a superposition of only even or odd modes and then simply adding the (even and odd) results together, as often done in determining the response of a simple shell to an applied load.

2.4. VIBRATIONAL POWER FLOWS INTO THE SUPPORTING SHELL

The power flow, say, through the jth isolator into the supporting shell can be obtained from

$$\mathbf{P}_j = \tfrac{1}{2}\,\Re\{\mathrm{i}w\tilde{\mathbf{R}}_j^{\mathrm{T}}\bar{\mathbf{U}}_j^*\}, \tag{35}$$

where $\Re$ and * denote the real part and complex conjugate of a complex variable respectively. Substituting equations (24) and (26) into equation (35) results in

$$\mathbf{P}_j = \sum_{\alpha=s,\theta,r}\mathbf{P}_{j\alpha} + \sum_{\substack{\alpha,\beta=s,\theta,r\\ \alpha\neq\beta}}\mathbf{P}_{j\alpha\beta}, \tag{36}$$

where

$$\mathbf{P}_{j\alpha} = \tfrac{1}{2}\Re\{\mathrm{i}\omega\tilde{\mathbf{R}}_{j\alpha}^{\mathrm{T}}\bar{\mathbf{U}}_{j\alpha}^*\}, \qquad \mathbf{P}_{j\alpha\beta} = -\tfrac{1}{2}\Re\{\mathrm{i}\omega\bar{\mathbf{U}}_{j\alpha}^{\mathrm{T}}\mathbf{Q}_j^{\mathrm{T}}\mathbf{K}_j\mathbf{Q}_j\bar{\mathbf{U}}_{j\beta}^*\} \tag{37, 38}$$

and

$$\tilde{\mathbf{R}}_{j\alpha} = \mathbf{Q}_j^{\mathrm{T}}\mathbf{K}_j\mathbf{G}_j\mathbf{u}^c - \mathbf{Q}_j^{\mathrm{T}}\mathbf{K}_j\mathbf{Q}_j\bar{\mathbf{U}}_{j\alpha}. \tag{39}$$

In equation (37), the quantity $\mathbf{P}_{j\alpha}$ represents the power flow (through the jth isolator) associated only with the displacement $\bar{\mathbf{U}}_{j\alpha}$, as though the other two displacements were zero. In contrast, the quantity $\mathbf{P}_{j\alpha\beta}$ in equation (38) represents the power flow corresponding to the cross coupling between any two different displacements. It is interesting that the power flows resulting from the cross coupling do not directly depend upon the motion of the machine. Experimentally, equation (36) may actually lead to an alternative technique (to the familiar impedance technique) for measuring the power transmission through isolators into the supporting structure.

The total or net power flow is the sum of the power flows through each of the isolators, namely,

$$\mathbf{P}_t = \sum_{j}^{N_k} \mathbf{P}_i = \mathbf{P}_{1t} + \mathbf{P}_{2t}, \tag{40}$$

where

$$\mathbf{P}_{1t} = \sum_{j}^{N_k} \sum_{\alpha=s,\theta,r} \mathbf{P}_{j\alpha}, \qquad \mathbf{P}_{2t} = \sum_{j}^{N_k} \sum_{\substack{\alpha,\beta=s,\theta,r \\ \alpha \neq \beta}} \mathbf{P}_{j\alpha\beta}. \tag{41, 42}$$

The total power flow is clearly a function of these variables used to describe the physical properties of the concerned components such as vibration isolators and the supporting shell. In addition, it is also dependent upon the locations of the vibration isolators with respect to the cylindrical shell. Therefore, in a vibration isolation design the total power can be conveniently used as a cost function to be minimized against any of these parameters.

It should be noted that although the current study has been focused on a simple cylindrical shell, other real-life structural features like reinforcing rings and beams can be readily taken into account without difficulties.

3. RESULTS AND DISCUSSIONS

Consider a machine mounted, via four identical vibration isolators, onto a circular cylindrical shell of radius $R = 0{\cdot}5$ m, length $L = 10R$ and thickness $h = 0{\cdot}02R$. The material properties for the shell are taken as: $E = 2{\cdot}07 \times 10^{11}$ N/m^2, $\nu = 0{\cdot}3$ and $\rho = 7800$ kg/m^3. The co-ordinates (x, θ), for the locations of the isolators are as follows: $(2R, \pi/12)$, $(2R, -\pi/12)$, $(4R, \pi/12)$, and $(4R, -\pi/12)$. The CG of the machine is located at $x = 3R$, $y = 0$ and $z = 1{\cdot}5R$. Other related model parameters are given in Table 1. For simplicity, a uniform modal damping, 1%, is assumed for the whole isolation system and an extra 2% hysteresis damping is added to the isolators. In all the following examples, the Fourier expansions are truncated to $M = 7$ and $N = 15$. Since the isolator spacing in the axial direction is roughly twice larger than that in the circumferential direction, more circumferential terms are chosen here so that the spatial resolutions will be about the same with respect to the wavelengths in both directions.

3.1. THE MODES FOR THE LOADED SHELL

To better understand the following discussions on power flows, let us first examine the modal modifications resulting from the addition of the machine and isolators to the shell.

TABLE 1

The properties of the machine, isolators and cylinder

Machine	Cylinder	Isolators
$m = 1000$ kg	$R = 0{\cdot}5$ m	$K_p = K_q = K_r = k_s = 3{\cdot}5 \times 10^6$ N/m
$I_{xx} = 102{\cdot}5$ kg/m^2	$L = 10R$	$K'_p = K'_q = K'_r = k_s/100$ N m/rad
$I_{yy} = 312{\cdot}5$ kg/m^2	$h = 0{\cdot}02R$	
$I_{zz} = 290$ kg/m^2		

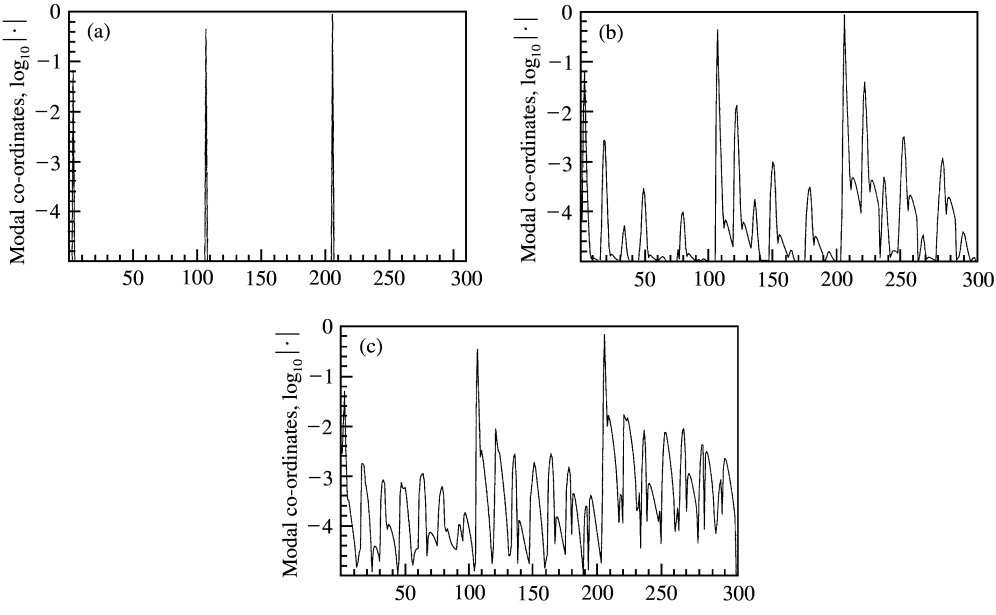

Figure 2. Modal co-ordinates for the (1, 2) mode and its counterparts: (a) $f_8 = 44{\cdot}48$ Hz, $k_s = 0$; (b) $f_8 = 49{\cdot}11$ Hz, $k_s = 3{\cdot}5 \times 10^6$ and (c) $f_2 = 30{\cdot}15$ Hz, $k_s = 3{\cdot}5 \times 10^9$.

The modal properties can be readily obtained from equation (34) by setting the (right-hand side) force vector to zero. It should be noted that all the elements in each eigenvector, except for those corresponding to the d.o.f.s for the machine, are actually the Fourier coefficients from which the traditional mode shape can be directly determined from equations (17). In Figures 2 and 3, two lower order shell modes are plotted for three different isolator stiffnesses, $k_s = 0, 3{\cdot}5 \times 10^6, 3{\cdot}5 \times 10^9$, which are, respectively, intended to represent the no/weak, moderate and strong coupling between the shell and the machine. A one-to-one mapping can be easily established between the Fourier coefficients and the components of an eigenvector. For example, the Fourier coefficients are arranged in Figures 2 and 3 as follows: $\{a_{10}, \ldots, a_{1n}, \ldots, a_{1N}, a_{20}, \ldots, a_{mn}, \ldots, a_{MN}, d_{11}, \ldots, d_{1n}, \ldots, d_{1N}, d_{21}, \ldots, d_{mn}, \ldots, d_{MN}, e_{10}, \ldots, e_{1n}, \ldots, e_{1N}, e_{20}, \ldots, e_{mn}, \ldots, e_{MN}\}$. Generally, there is a total of $6MN - 3M$ Fourier coefficients. However, due to the symmetric nature of these two modes, all the Fourier coefficients corresponding to the asymmetric terms are virtually zero. For $k_s = 0$, the motions of the shell and rigid body become completely independent and each mode is simply represented by three vertical lines from whose positions its modal indices, (m, n), can be easily identified. It should be noticed that even if the lower order modes for a thin shell can often be characterized as *primarily radial* (refer to the (1, 1) mode in Figure 2(a)), it does not necessarily suggest that the radial displacement is always dominant (refer to the (1, 1) mode in Figure 3(a)). As seen later, this clarification will help to explain why it may not be sufficient to only consider the radial displacement in power flow calculations. For a moderate isolator stiffness such as $k_s = 3{\cdot}5 \times 10^6$, the presence of the machine will have a certain influence on the modal behaviors for the simple shell. However, the modal modifications are typically manifested in the slight shifts of natural frequencies and minor distortions to the original mode shapes. For a very large isolator stiffness such as $k_s = 3{\cdot}5 \times 10^9$, the shell and machine are virtually joined together and the machine behaves more like a mass loading to the shell. Consequently, the new modes become much more complicated and unpredictable.

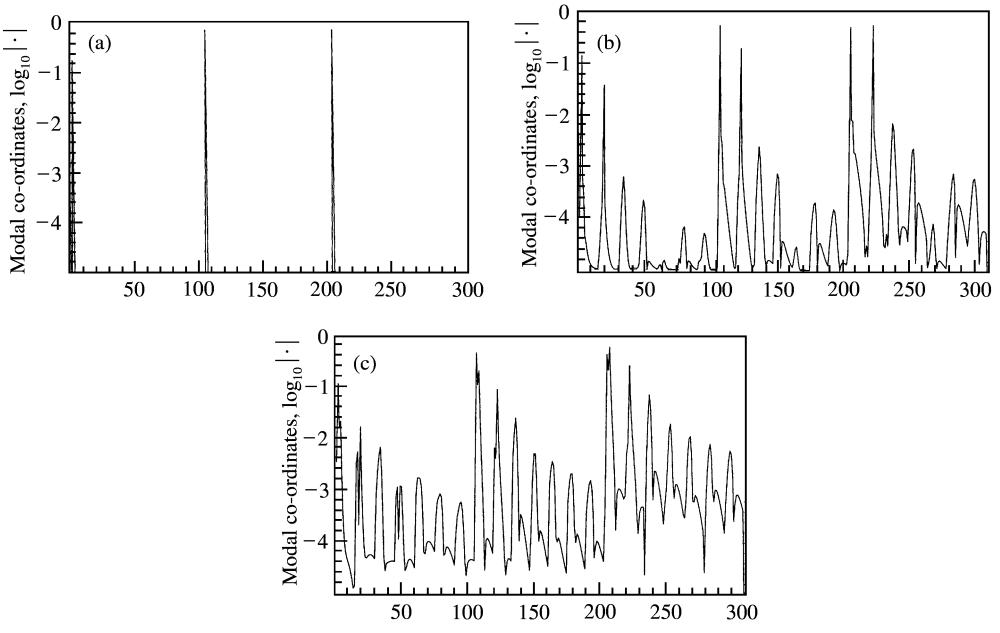

Figure 3. Modal co-ordinates for the (1, 1) mode and its counterparts: (a) $f_{11} = 101{\cdot}6$ Hz, $k_s = 0$; (b) $f_{11} = 102{\cdot}2$ Hz, $k_s = 3{\cdot}5 \times 10^6$ and (c) $f_8 = 92{\cdot}62$ Hz, $k_s = 3{\cdot}5 \times 10^9$.

3.2. VIBRATIONAL POWER FLOWS INTO THE SUPPORTING SHELL

Suppose the machine is subject to a vertical force, $F_z = \omega^2$ N. This particular form of spectrum is simply chosen to reduce the dynamic range of the response variables such as the power flows into the supporting shell. The curves in Figure 4 show the total or net powers transmitted through four isolators ($k_s = 3{\cdot}5 \times 10^6$) into the supporting shell. While the solid line has considered the contributions of all three displacement components, the dash curve has only accounted for the contribution of the radial displacement. It is seen that in this particular case, the radial vibration of the shell has played a dominant role in conveying the vibrational powers. This outcome, however, should not come as a surprise. In view of the manner in which the external force is applied, one can intuitively expect that the reaction forces at the isolator locations will be primarily in the vertical (or almost radial) directions. Since the power flows depend upon both the reaction forces and the velocities at the isolator locations, the "primarily radial" motions plus predominantly radial forces dictate the (power transmission) characteristic observed in Figure 4. However, this observation should not be perceived as a general testimony because there is no guarantee that the reaction forces are always predominantly in the radial directions. This will become clear from the following examples.

Now, consider a transverse force, $F_y = \omega^2$ N, is applied to the machine. Figure 5 shows the total power flows associated with the radial, tangential and all three displacements. The power flow associated with the axial displacement is not plotted simply because of its insignificance. Intutitively, for this load condition the reaction forces will essentially exert a primarily transverse or tangential force on the shell. Unlike the previous example, it is clearly inadequate here to only take into account the radial displacement. This notion is also true for some other non-radial-only load conditions, for example, when a moment, $M_x = \omega^2$ N m, about the x-axis is applied. The corresponding power flow curves are given

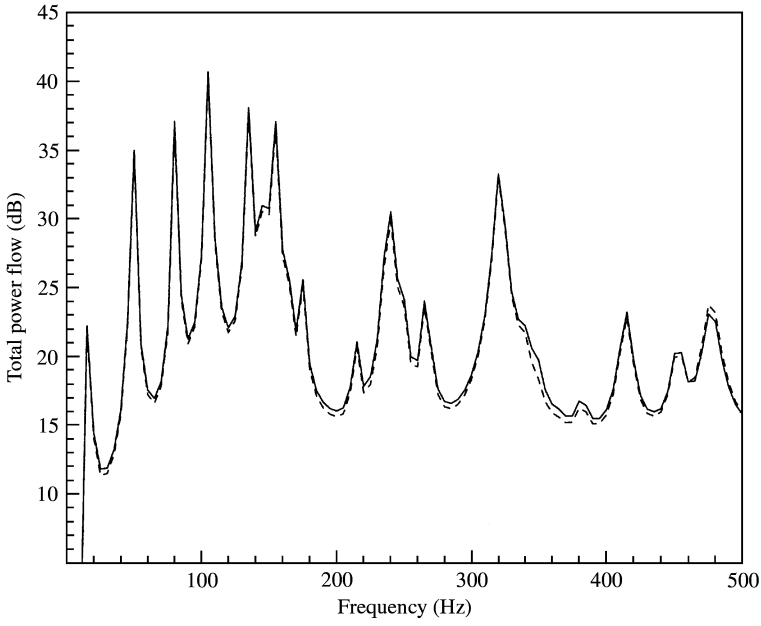

Figure 4. Total power flows (in dB ref. 1 W): ——, equation (40); - - - -, due to radial displacement only; $F_z = \omega^2$ N.

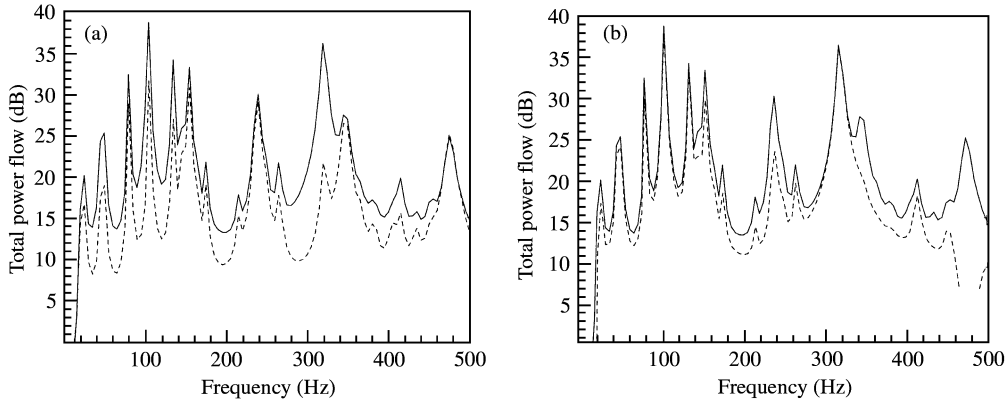

Figure 5. Total power flows (in dB ref. 1 W): ——, equation (40); (a) - - - -, due to radial displacement; (b) – – – –, due to transverse displacement; $F_y = \omega^2$ N.

in Figure 6. Intuitively, for this load condition the resultant reaction forces approximately consist of a transverse force, a vertical force and a moment about x-axis. While the transverse force primarily sustains the power flow associated with the circumferential displacement, the other two predominantly maintain the power flows associated with the flexural motions. Again, due to the way in which the load is applied, the power flow associated with the axial displacement is substantially small and is not shown here.

It has been observed in the last two examples that only consideration of the radial displacement or flexural motions cannot accurately determine the power flows from

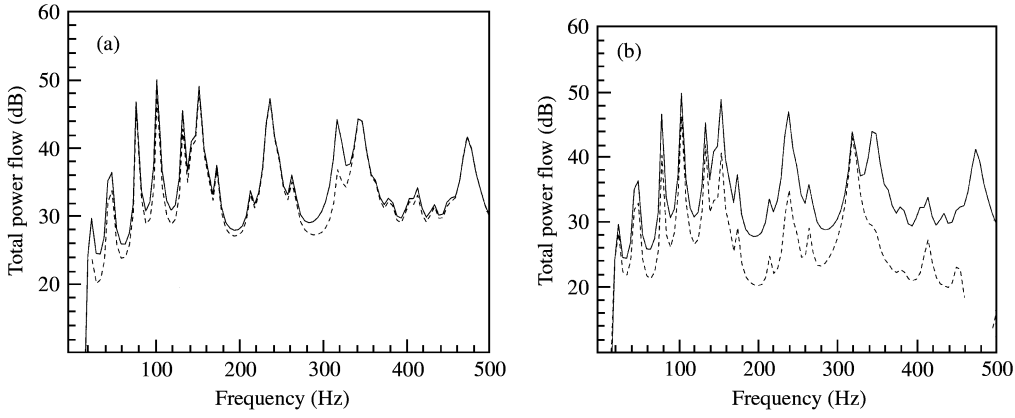

Figure 6. Total power flows (in dB ref. 1 W): ——, equation (40); (a) - - - -, due to radial displacement; (b) – – – –, due to transverse displacement; $M_x = \omega^2$ N m.

a vibratory machine to its supporting structure. Even though a qualitative characterization of the reaction forces has been attempted in each of the previous load cases, it may not be always possible for many real-world problems which are often less ideal with respect to isolator arrangement, the inertial matrix of a machine, loading condition, and so on. Therefore, it is risky to automatically assume that only the radial displacement or flexural motions are important in coveying vibrational powers to a machine supporting structure.

3.3. THE EFFECTS OF THE CROSS COUPLING OF DISPLACEMENTS

So far, the discussions have been focused on the contributions to power flows of the radial and non-radial displacement components. A further examination indicates that the power flows resulting from the cross coupling of different displacements are essentially meaningless in all the three examples. Because this observation is not sensitive to the load conditions, one has to turn to other model variables to see the effects, if any, of the cross coupling of the displacements. Intuitively, one can expect that the degree of the cross coupling between any two displacements will increase with isolator stiffness. Accordingly, let us now specify the isolator stiffness as $k_s = 3{\cdot}5 \times 10^9$. This may be considered as a case, for example, when the machine is rigidly mounted onto the shell through a set of bolts instead of vibration isolators. In order to understand the importance of the cross coupling, the power flows calculated in various manners are compared in Figure 7 for $F_y = \omega^2$ N and in Figure 8 for the simultaneous action of $F_y = \omega^2$ N and $M_x = \omega^3$ N m. It is seen that in both cases the power flows, P_{1t}, determined without considering the effects of the cross coupling are essentially not acceptable at low frequencies. The missing portions of the curves indicate negative power flows (that is, from the supporting structure to the source machine) at the corresponding frequencies. Although the total or net power always flows from the source machine to the receiving structure, the partial power flows, P_{1t} and P_{2t}, can go in any direction. At a given frequency (e.g., 20 Hz), the contribution from the cross coupling exceeding the total power suggests that the same amount of power, P_{1t}, is conveyed back to the machine. One should also notice that the power flow, P_{2t}, resulting from the cross coupling becomes less important at higher frequencies, and approximately levels off as frequency further increases.

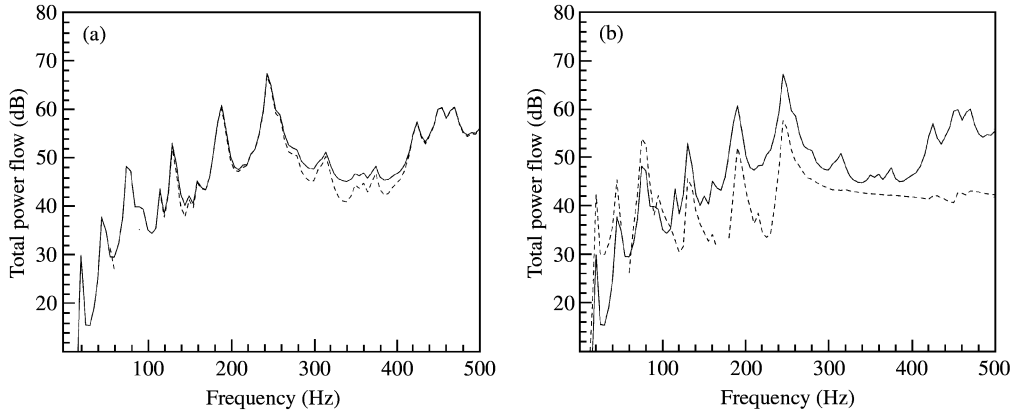

Figure 7. Total power flows (in dB ref. 1 W): ——, equation (40); (a) - - - -, no cross coupling, equation (41); (b) - - - -, only due to cross coupling, equation (42); $k_s = 3{\cdot}5 \times 10^9$; $F_y = \omega^2$ N.

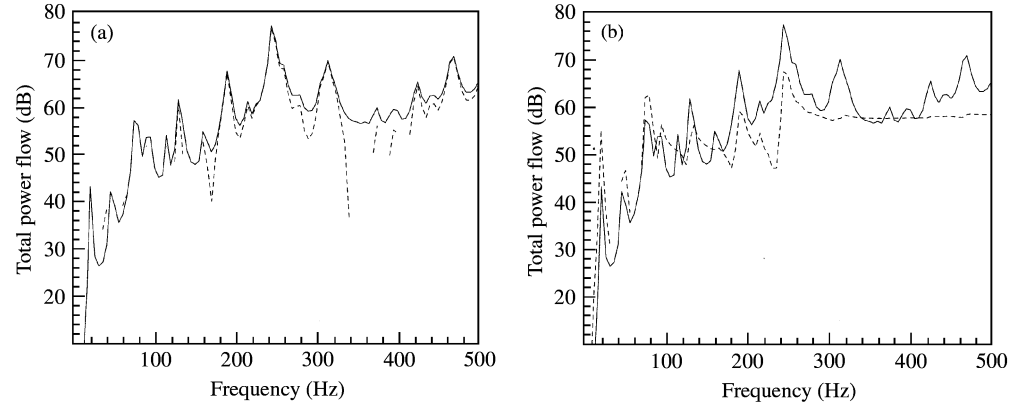

Figure 8. Total power flows (in dB ref. 1 W): ——, equation (40); (a) - - - -, no cross coupling, equation (41); (b) - - - -, only due to cross coupling, equation (42); $k_s = 3{\cdot}5 \times 10^9$; $F_y = \omega^2$ N and $M_x = \omega^2$ N m.

4. CONCLUSIONS

Vibrational power flows from a source machine into its supporting cylindrical shell are studied with consideration of both the radial and non-radial motions of the shell. The vibrations of the shell are determined from the Goldenveizer–Novozhilov (or Arnold–Warburton) equations that are usually considered more accurate than the popular Donnell–Mushtari equations, especially for shells with a large length-to-radius ratio. The complete Fourier expansions (consisting of both symmetric and asymmetric terms) of the displacements in the circumferential direction allow a correct prediction of power flows for complex isolation systems involving, say, a non-symmetric mass matrix, a general isolator placement plan, and/or complicated load conditions. It is emphasized that the primarily radial motion of a thin shell does not necessarily dictate that the vibrational power transmission is predominantly carried out by the radial displacement, such that only the flexural motion needs to be taken into consideration. This notion is subsequently reinforced by numerical results which clearly indicate that the non-radial displacements can be as

important as the radial displacement in transferring vibrational powers to a supporting shell.

Another issue discussed is concerned with the effects on the power flows of the cross coupling of the displacement components. When the vibration isolators are sufficiently soft, the cross coupling appears to have a negligible impact on the power flows. However, it is numerically demonstrated that for very stiff isolators (or more appropriately, connectors), the power flows resulting from the cross coupling can become meaningfully important, especially at low frequencies. From an analytical point of view, the consideration of the cross coupling will not add any significant difficulties to the power flow calculations. However, it may become critical if power flows are to be measured experimentally.

REFERENCES

1. Y. K. KOH and R. G. WHITE 1996 *Journal of Sound and Vibration* **196**, 469–493. Analysis and control of vibrational power transmission to machinery supporting structures subjected to a multi-excitation system. Part I: driving point mobility matrix of beams and rectangular plates.
2. Y. K. KOH and R. G. WHITE 1996 *Journal of Sound and Vibration* **196**, 495–508. Analysis and control of vibrational power transmission to machinery supporting structures subjected to a multi-excitation system. Part II: vibrational power analysis and control schemes.
3. Y. K. KOH and R. G. WHITE 1996 *Journal of Sound and Vibration* **196**, 509–522. Analysis and control of vibrational power transmission to machinery supporting structures subjected to a multi-excitation system. Part III: vibrational power cancellation and control experiments.
4. R. J. PINNINGTON and R. G. WHITE 1981 *Journal of Sound and Vibration* **68**, 179–197. Power flow through machine isolators to resonant and non-resonant beams.
5. H. G. D. GOYDER and R. G. WHITE 1980 *Journal of Sound and Vibration* **68**, 59–75. Vibrational power flow from machines into built-up structures. Part I: introduction and approximate analyses of beam and plate-like foundations.
6. H. G. D. GOYDER and R. G. WHITE 1980 *Journal of Sound and Vibration* **68**, 77–96. Vibrational power flow from machines into built-up structures. Part II: wave propagation and power flow in beam-stiffened plates.
7. H. G. D. GOYDER and R. G. WHITE 1980 *Journal of Sound and Vibration* **68**, 97–117. Vibrational power flow from machines into built-up structures. Part III: power flow through isolation systems.
8. J. PAN, J. Q. PAN and C. H. HANSEN 1997 *Journal of the Acoustical Society of America* **92**, 895–907. Total power flow from a vibrating rigid body to a thin panel through multiple elastic mounts.
9. C. Q. HOWARD, J. Q. PAN and C. H. HANSEN 1997 *Journal of the Acoustical Society of America* **101**, 1479–1491. Power transmission from a vibrating body to a circular cylindrical shell through active elastic isolators.
10. W. L. LI and P. LAVRICH 1999 *Journal of Sound and Vibration* **224**, 757–774. Prediction of power flows through machine vibration isolators.
11. P. GARDONIO, S. J. ELLIOTT and R. J. PINNINGTON 1997 *Journal of Sound and Vibration* **207**, 61–93. Active isolation of structural vibration on a multiple-degree-of-freedom system. Part I: the dynamics of the system.
12. P. GARDONIO, S. J. ELLIOTT and R. J. PINNINGTON 1997 *Journal of Sound and Vibration* **207**, 95–121. Active isolation of structural vibration on a multiple-degree-of-freedom system. Part II: effectiveness of active control strategies.
13. M. A. SANDERSON 1996 *Journal of Sound and Vibration* **198**, 171–191. Vibration isolation: moments and rotations included.
14. B. A. T. PETERSSON 1993 *Journal of Sound and Vibration* **160**, 43–66. Structural acoustic power transmission by point moment and force excitation. Part I: beam- and frame-like structures.
15. B. A. T. PETERSSON 1993 *Journal of Sound and Vibration* **160**, 67–91. Structural acoustic power transmission by point moment and force excitation. Part I: plate-like structures.
16. B. A. T. PETERSSON and B. A. GIBBS 1993 *Journal of Sound and Vibration* **168**, 157–176. Use of the source descriptor concept in studies of multi-point and multi-directional vibrational sources.
17. A. LEISSA 1993 *Vibration of Shells*. Acoustical Society of America.
18. W. SOEDEL 1993 *Vibrations of Shells and Plates*. New York: Marcel Dekker, Inc.

APPENDIX A: THE DEFINITIONS OF THE SUB-MATRICES

The elements of the sub-matrices in equations (19) are defined as follows:

$$\Lambda^{ss}_{mn,m'n'} = \delta_{mm'}\delta_{nn'}(1+\delta_{n0})\varpi^2 m_s\left[\frac{(1-\nu)}{2}n^2 + \lambda_m^2\right], \tag{A1}$$

$$\Lambda^{s\theta}_{mn,m'n'} = -\delta_{mm'}\delta_{nn'}(1+\delta_{n0})\varpi^2 m_s\left[\frac{(1+\nu)}{2}n\lambda_m\right], \tag{A2}$$

$$\Lambda^{sr}_{mn,m'n'} = -\delta_{mm'}\delta_{nn'}(1+\delta_{n0})\varpi^2 m_s \nu\lambda_m, \tag{A3}$$

$$\Lambda^{\theta\theta}_{mn,m'n'} = \delta_{mm'}\delta_{nn'}(1+\delta_{n0})\varpi^2 m_s\left[n^2 + \frac{(1-\nu)}{2}\lambda_m^2 + \kappa n^2 + 2\kappa(1-\nu)\lambda_m^2\right], \tag{A4}$$

$$\Lambda^{\theta r}_{mn,m'n'} = \delta_{mm'}\delta_{nn'}(1+\delta_{n0})\varpi^2 m_s[n + \kappa n^3 + (2-\nu)\kappa n\lambda_m^2], \tag{A5}$$

$$\Lambda^{rr}_{mn,m'n'} = \delta_{mm'}\delta_{nn'}(1+\delta_{n0})\varpi^2 m_s(1 + \kappa n^4 + 2\kappa n^2\lambda_m^2 + \kappa\lambda_m^4), \tag{A6}$$

$$\bar{p}^s_{s,mn} = \int_0^{L/R}\int_0^{2\pi} p_s(s,\theta)\cos\lambda_m s\cos n\theta\,\mathrm{d}\theta\,\mathrm{d}s, \tag{A7}$$

$$\bar{p}^s_{\theta,mn} = \int_0^{L/R}\int_0^{2\pi} p_\theta(s,\theta)\sin\lambda_m s\sin n\theta\,\mathrm{d}\theta\,\mathrm{d}s, \tag{A8}$$

$$\bar{p}^s_{r,mn} = \int_0^{L/R}\int_0^{2\pi} p_r(s,\theta)\sin\lambda_m s\cos n\theta\,\mathrm{d}\theta\,\mathrm{d}s, \tag{A9}$$

$$p^a_{s,mn} = \int_0^{L/R}\int_0^{2\pi} p_s(s,\theta)\cos\lambda_m s\sin n\theta\,\mathrm{d}\theta\,\mathrm{d}s, \tag{A10}$$

$$\bar{p}^a_{\theta,mn} = \int_0^{L/R}\int_0^{2\pi} p_\theta(s,\theta)\sin\lambda_m s\cos n\theta\,\mathrm{d}\theta\,\mathrm{d}s, \tag{A11}$$

$$\bar{p}^a_{r,mn} = \int_0^{L/R}\int_0^{2\pi} p_r(s,\theta)\sin\lambda_m s\sin n\theta\,\mathrm{d}\theta\,\mathrm{d}s, \tag{A12}$$

where

$$\varpi^2 = \frac{E}{\rho(1-\nu^2)R^2}. \tag{A13}$$

APPENDIX B: NOMENCLATURE

$a_{mn}, b_{mn}, c_{mn}, d_{mn}, e_{mn}, f_{mn},$	Fourier expansion coefficients
E	Young's modulus
f	external forces applied to the machine

$\mathbf{G}_i$	transformation matrix
h	shell thickness
$I_{xx}, I_{xy}, I_{xz}, \ldots, I_{zy}, I_{zz}$	moments of inertia of the source machine
$\mathrm{i} =$	$(-1)^{1/2}$
$\bar{\mathbf{K}}$	global stiffness matrix
$\mathbf{K}_i$	stiffness matrix of the ith isolator
$\mathbf{K}_i^g =$	$\mathbf{G}_i^{\mathrm{T}}\mathbf{K}_i$
K_i^p, K_i^q, K_i^r	linear stiffnesses in the principal directions of the ith isolator
$K_i'^p, K_i'^q, K_i'^r$	rotational stiffnesses in the principal directions of the ith isolator
L	length of a cylindrical shell
$\mathbf{M}$	mass matrix
M, N	numbers of expansion terms used in s and θ direction respectively
m	mass of a rigid-body machine
P_j	power flow through the ith isolator
P_t	total power flow through all isolators
P_{t1}	total power flow calculated without considering the cross coupling
P_{t2}	total power flow resulting from the cross coupling
p_s, p_θ, p_r	distributed forces in $s\ (= x/R)$, θ and r directions
$\mathbf{Q}_i, \hat{\mathbf{Q}}_i$	co-ordinate transformation matrices
$\mathbf{R}_i$	reaction force at the ith isolator location
$\tilde{\mathbf{R}}_i$	reaction force at the ith isolator location in cylindrical co-ordinate system
$\mathbf{R}_i^c$	load due to the reaction force at the ith isolator location
R	shell radius
$s =$	x/L
$\mathbf{T}_i, \hat{\mathbf{T}}_i$	co-ordinate transformation matrices
$\bar{\mathbf{U}}_i$	displacements at the ith isolator in the cylindrical co-ordinate system
$\mathbf{u}_i, \mathbf{u}_i^0$	displacement vectors at the upper and lower ends of the ith isolator
$\mathbf{u}^c$	displacement vector of the center of gravity of the source machine
u, v, w	axial, transverse (or circumferential) and radial displacements
x, θ, r	cylindrical co-ordinates
δ_{mn}	Kronecker delta function
$\delta(x, y)$	delta function
$\kappa =$	$h^2/12R^2$
$\lambda_m =$	$m\pi R/L$
ν	the Poisson ratio
ρ	mass density
ω	frequency in radian
$\varpi^2 =$	$\dfrac{E}{\rho(1-\nu)R^2}$